Folic acid and sodium folate salts: Thermal behavior and spectroscopic (IR, Raman, and solid-state 13C NMR) characterization

Vagner Magri, Michele Rocha, Caroline S. de Matos, Philippe A.D. Petersen, Fabrice Leroux, Helena Petrilli, Vera R.L. Constantino

Folic Acid and Sodium Folate Salts: Thermal Behavior and Spectroscopic (IR, Raman, and Solid-state ^{13}C-NMR) Characterization

Vagner R. Magri,[a] Michele A. Rocha,[a] Caroline S. de Matos,[a] Philippe A. D. Petersen,[b] Fabrice Leroux ,[c,d] Helena M. Petrilli[b] and Vera R. L. Constantino[a*]

[a]Departamento de Química Fundamental, Instituto de Química, Universidade de São Paulo, Av. Prof. Lineu Prestes 748, CEP 05508-000, São Paulo, SP, Brazil

[b]Departamento de Física de Materiais e Mecânica, Instituto de Física, Universidade de São Paulo, Rua do Matão 1371, CEP 05508-090, São Paulo, SP, Brazil

[c]Université Clermont Auvergne, Institut de Chimie de Clermont-Ferrand, BP 10448, F-63000 Clermont-Ferrand, France

[d]CNRS, UMR 6296, ICCF, F-63178 Aubiere, France.

* Corresponding author.
E-mail address: vrlconst@iq.usp.br (V.R.L. Constantino)

KEYWORDS
Folic Acid, Sodium Folate Salts, Pteroyl-L-glutamic acid, vitamin B9, DFT

HIGHLIGHTS

- The main spectroscopic signatures of Folic acid, Na_2Folate (dianionic) and Na_3Folate (trianionic) compounds were highlighted, as well as the influence of the protonation level in their physicochemical properties.
- Spectroscopic data interpretation was supported by theoretical calculations.
- The compounds were also characterized by UV-VIS diffuse-reflectance spectroscopy, thermal analysis (TG/DTG-DSC-MS), and X-ray diffractometry.

GRAPHICAL ABSTRACT

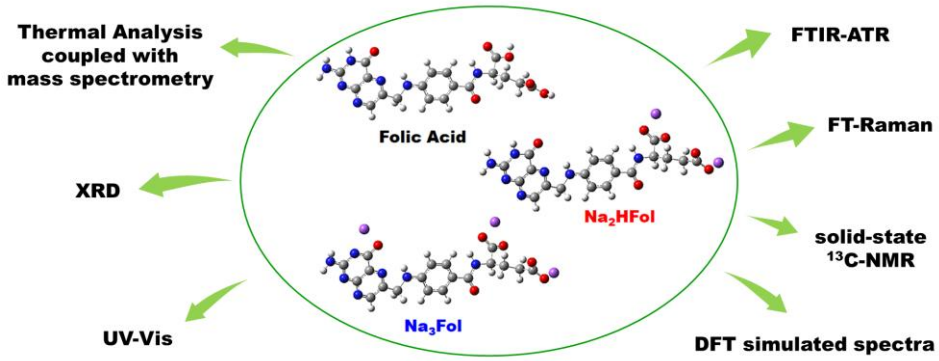

ABSTRACT

Folic acid (FA; vitamin B9) and its associated sodium salts, strongly relevant for many scientific and technological applications - from nutrition to pharmacology and nanomedicine, suffer from a lack of characterization combining experimental and theoretical. In this work, a spectroscopic investigation of FA and its synthesized sodium salts in the form of dianion (Na_2HFol) or trianion (Na_3Fol) was scrutinized in their solid state. The spectroscopic (infrared, Raman, and solid state ^{13}C-nuclear magnetic resonance) data interpretation was supported by theoretical calculations using the Density Functional Theory (DFT). Additionally, the compounds were characterized by UV-VIS diffuse-reflectance spectroscopy, combined thermal analyses (TG/DTG-DSC) coupled to mass spectrometry, and X-ray diffractometry. The main signatures of each species were identified, as well as the influence of the protonation level on their physicochemical properties. These distinct properties for the three compounds are mainly based on signals assigned to glutamic acid (glutamate) and pterin (neutral and anionic) moieties. This work should help developing new products based on FA or its anionic forms, such as theragnostic/drug delivery systems, supramolecular structures, nanocarbons, or metal complexes.

1. Introduction

Scientific, clinical, and public health interests concerning folic acid (FA; Pteroyl-L-glutamic acid) have long been established. The importance of FA and its anionic species in food engineering, pharmacology, nanotechnology, and nanomedicine, among other fields is undeniable. The global market of FA production has been estimated at around half a billion dollar per year with an increasing prospect [1]. The list of uses for FA is extensive, mostly because its chemical composition and molecular structure. As illustrated in **Figure 1a**, the FA molecule is constituted by three distinct moieties: pterin (PT), *p*-aminobenzoic acid (*p*-ABA) and L-glutamic acid (Glu).

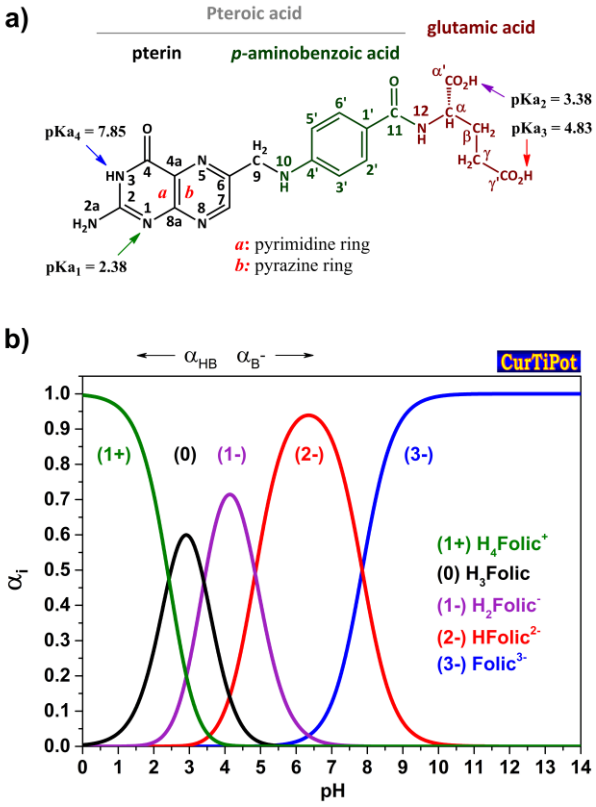

Figure 1. a) Molecular structure of FA and its apparent dissociation constants (pK_a's values), as determined by Szakács and Noszál [2]; b) Chemical speciation of FA in the range of pH values from 0 to 14, obtained by CurTiPot software.

FA is the basic structural synthetic analogue and the most oxidized form of the essential micronutrients group commonly termed as folates and vitamin B_9 [3,4]. Folates act as enzymatic cofactors in a set of cellular biochemical reactions denominated as

one-carbon (1C) metabolism [5,6], and are necessary for the proliferation of cells, genic expression control and in the maintenance of the cellular redox balance [5,6]. Furthermore, FA presents antioxidant properties [7,8] and prevents inflammation, which can lead to endothelial dysfunction [8] and cognitive impairment/dementia [9]. FA consumption is encouraged in several countries to fight against malnutrition and strengthen the little ones, especially birth defects as FA-sensitive neural tube defects [10,11]. FA is taken orally using diverse drugs formulations [12], as well as some products containing FA and iron(II) complexes recommended as antianemia drugs by the United Nations Children's Fund (UNICEF), in line with the World Health Organization (WHO) [13].

The sustained release of FA is also reported in innovative formulations in cosmetics [7,14]. In nanomedicine field, studies focused on harnessing the power of FA as a targeting agent for imaging and/or therapy (theragnosis) of cancer and inflammatory diseases [15–18]. The nanoengineering of smart delivery systems includes plenty of organic and inorganic nanoparticles as well as FA-drug conjugates [16–18]. In addition, FA forms complexes with a series of metal cations by coordination with its Glu or PT moieties [19–24]. Such complexes can be used as antimicrobial agent [19,23], anticancer-drug [24] or in the treatment of diabetes [22]. In nanomaterial and nanotechnology science, FA has been used as precursor of supramolecular structures (liquid crystals and gels) [25–27] and nitrogen doped carbonaceous materials [27,28]. The development of photoelectric devices containing FA is envisaged because of its electronic properties [29].

Spectroscopic analyses combined with theoretical calculations using the Density Functional Theory (DFT) are powerful tools to characterize organic compounds and nanomaterials. Despite their very wide applicability, only a limited number of studies

on FA following this approach are reported in the literature. Studies use crystalline FA as the standard, performing experimental infrared (IR) and/or Raman spectroscopies, and interpret the results by combining with theoretical DFT calculations. Most works focus on the FA analysis by Surface-enhanced Raman scattering (SERS) spectroscopy because its promising use in analyses of biological samples. In general, the studies investigate the influence of the temperature and substrate (gold or silver) on the SERS spectral profile of FA [30] as well as the adsorption mechanism of FA onto different substrates [31–33]. Furthermore, the photodegradation (under UV) [34] and the hydrothermal decomposition [35] of FA is inspected by a spectroscopic approach combining experimental and theoretical data.

The solubility of neutral FA is low (0.1069 mmol kg^{-1} at 25 ºC, 1 bar and pH = 4.28) [36] and pH-dependent in water. It is significantly increased in pH values above 5 [37], for which the dianion ($HFol^{2-}$) and trianion (Fol^{3-}) are then dominant species [2] (**Figure 1b**). Therefore, folate anionic species which studies are often neglected must nevertheless be considered because of: (*i*) at physiological pH value for which $HFol^{2-}$ is predominant [38–40]; (*ii*) the preparation of many materials and compounds (or the handle of FA in some studies) are performed at pH values above 5 [7,14,22–24,31–34]; and (*iii*) the supramolecules assembled by FA are pH-responsiveness [25–27]. Braga et al. [41] prepared dianionic folates salts (Li, Na and Ca) and showed their higher dissolution rate as well as higher thermal stability than FA. However, the experimental and theoretical spectroscopic analyses of folate salt are not accomplished yet. Gocheva et al. [38] studied the tautomerism of dianion folate ($HFol^{2-}$) in water by ^{1}H- and ^{13}C-NMR and interpreted the results based on DFT calculations with the Polarizable Continuum Model (PCM). Experimental and calculated IR spectra of palladium and

platinum folate complexes were reported by He et al. [24], but the theoretical (DFT) values and the correlated attribution were not presented.

The knowledge of physical-chemical features of FA and its salts in the solid state by usual laboratory techniques is essential and useful because contribute to the development of new products, combined to a more assertive characterization of their properties. Our group has performed the thermal and spectroscopic characterizations of bioactive molecules and their respective sodium salts [42–44]. In this study, the spectroscopy profile (IR, Raman, and solid state ^{13}C-NMR) of solid FA (commercial) is compared to its synthesized sodium salts used as a model of dianion (Na_2HFol) and trianion (Na_3Fol) forms of FA. The main signatures of each species are tracked as well as the influence of the protonation level in their physicochemical properties. The spectroscopic analyses are supported by theoretical calculations using DFT. The samples are also characterized by UV-VIS diffuse-reflectance spectroscopy, thermal analysis (TG/DTG-DSC-MS), and X-ray diffractometry. To the best of our knowledge, this is the first study comparing consistently the physical-chemical features of FA and its sodium salts in their solid-state. In addition, this work gives us the opportunity to compare data already published on FA.

2. Materials and Methods

2.1. Preparation of folate sodium salts

FA ($C_{19}H_{19}N_7O_6$, ≥ 97%) from Sigma-Aldrich and standard aqueous sodium hydroxide 0.1 mol·L^{-1} solution from Merck were used as received. Na_2HFol and Na_3Fol samples were prepared by the stoichiometric reaction between 0.7 g of FA and the standard 0.1 mol L^{-1} NaOH aqueous solution and further isolated by lyophilization process using Thermo Savant ModulyoD equipment (200 mPa and -50 ºC).

2.2. Physical Measurements

X-ray diffraction (XRD) patterns of powdered samples were recorded on a Bruker diffractometer model D8 DISCOVER, equipped with Nickel-filtered CuKα radiation (0.15418 nm), operating at 40 kV and 30 mA, sample rotating at 30 rpm, and collected in the (2 θ) 5–70 ° range, with steps of 0.05 °/2θ and scan speed of 0.05 °/3 s.

Diffuse reflectance spectra (Kubelka-Munk) of solid samples in the UV-VIS region were recorded in a Shimadzu model UV-2401PC spectrophotometer, equipped with an integration sphere. $BaSO_4$ (Waco Pure Chem.) was used to dilute the samples. FA titration was carried out in aqueous media (0.024 mmol·L^{-1}) using NaOH aqueous solution (0.10 mol·L^{-1}) and the UV-VIS electronic spectra of the resulting solutions were registered in a Shimadzu UV-1650PC spectrophotometer.

Thermal Analysis (TG/DTG-DSC-MS) were conducted on a Netzsch thermoanalyzer, model TGA/DSC 490 PC Luxx, coupled to Aeolos® 403 C Quadro mass spectrometer, from room temperature to 1000 ^oC, under compressed air flow (50 mL·min^{-1}), using heating rate of 10 °C·min^{-1} and an alumina crucible. Differential Scanning Calorimetry (DSC) data under N_2 flow (50 mL·min^{-1}) were obtained from

room temperature to 380 ^{o}C, using a heating rate of 10 °C·min^{-1}. The sample modifications that occur during heating were also evaluated in a Melting point apparatus from Microquimica, model MQAPF – 302, operating in a heating rate of 10 °C·min^{-1}; the powdered sample was sandwiched between cover glasses and placed on the heating block. During the analysis, the sample was illuminated by a lamp and transformations could be visualized by magnifying lens.

The Fourier transform infrared (FTIR) spectra were recorded in a Bruker Alpha spectrophotometer (DTGS detector and KBr optics), using a single bounce Attenuated Total Reflectance (ATR) accessory equipped with a diamond crystal, in the 4000–400 cm^{-1} range with spectral resolution of 4 cm^{-1} and 512 scans. Data were collected on the absorbance mode and manually converted to transmittance. Raman spectra were recorded in a Bruker FT-Raman instrument, model MultiRam, equipped with Ge detector (cooled by liquid nitrogen) and Nd^{3+}/YAG laser (1064 nm exciting radiation), in the range of 3500-100 cm^{-1} with 4 cm^{-1} of spectral resolution and 1024 scans, using 150 mW power on the samples.

^{13}C (I = 1/2) solid state nuclear magnetic resonance (NMR) analysis was performed on Bruker Advance 300 MHz using magic angle spinning (MAS) at 10 kHz and a 4 mm diameter size zirconia rotor. ^{13}C spectra were obtained by ^{1}H enhanced cross-polarization method (CP, contact time of 1 ms, recycling time of 5 s). Calibration was made using carbonyl group of glycine as reference (176.03 ppm) and 2,000 to 10,000 scans were needed to obtain a proper signal for samples.

2.3. Theoretical Methods

Calculations in the Kohn-Sham (KS) scheme of the Density Functional Theory (DFT) were performed to obtain geometry optimizations, vibrational (IR and Raman)

and NMR chemical shifts, for FA and sodium folates (Na_2HFol and Na_3Fol). All geometries presented in this paper were obtained in a gas phase environment simulation and the B3LYP hybrid functional with the 6-311++G(d,p) Gaussian basis sets were employed [45,46]. The Gaussian09 software package was used for geometry optimizations, vibrational spectra acquisition, and NMR calculations [47]. Structural optimizations were performed considering the X-ray diffraction data of FA single crystal as reference [48]. The theoretical infrared and Raman spectra (wavenumbers and intensities/activities) were acquired at the same level of theory as the geometry optimizations. The spectra were shown with a resolution of 1 cm^{-1} and applying a 0.975 scaling factor from 4000 to 1000 cm^{-1} to correct the anharmonicity effects on the vibrational spectra [49].

3. Results and Discussion

The neutral PT moiety exists in different tautomeric forms while the anion form has different mesomers [38,50], as reviewed in Appendix A–Supplementary Material (**SM**). The neutral PT (as in FA and $HFol^{2-}$ ion) exhibits a keto-enol (lactam-lactim) equilibrium between C4=O and N3–H groups (see **Figure A.1** in **SM**), and the keto form has two tautomers, comprising the hydrogen atom bonded to N3 or N1 atoms. Anionic PT (as in $Folate^{3-}$) presents mesomer resonance structures as amidate ($^{-}$N3–C4=O) and enolate (N3=C4–O^{-}), as also shown in **Figure A.1**. In this work, the 3-lactam tautomer (**Figure 1a**) for FA and Na_2HFol samples, as well as the enolate mesomer form for Na_3Fol sample, were considered the main forms of PT based on stability data reviewed in **Section 1** of **SM**.

3.1. X-ray diffractometry and UV−VIS spectroscopy

The XRD patterns of powdered compounds are presented in **Figure 2**. Commercial FA presents XRD profile typical of a crystalline compound with some intense diffraction peaks observed at 2θ values of 5.51°, 10.97º and 13.18°. From Vesta software [51] and using the CIF from Ref. [52] (CCDC N 1489544), such peaks are assigned to the diffraction plans (002), (004) and (013), respectively. These results are in agreement with those reported for the dihydrate FA (primitive orthorhombic unit cell and space group $P2_12_12_1$) [41,48,52]. Kaduk, Crowder and Zhong [52] re-determined the structure of dihydrate FA using synchrotron X-ray diffraction analysis, Rietveld refinement techniques and DFT calculations. In the crystal (**Figure A.2**), the Glu chain exists in a bent conformation while *p*-ABA and PT moieties are slightly tilted relative to each other. The molecules in the crystal are networking by intermolecular H-bonds and the pyrimidine and benzene rings of adjacent molecules are stacked at around 0.34 nm (**Figure A.2**).

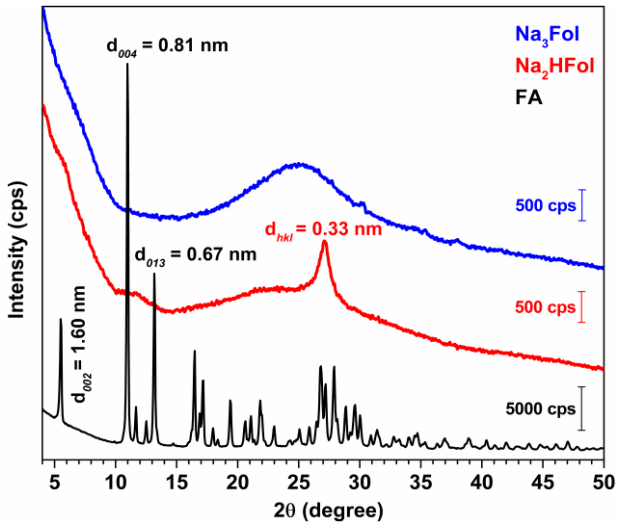

Figure 2. XRD patterns of dihydrate FA (commercial sample), and the Na_2HFol and Na_3Fol salts prepared in this work.

The XRD patterns of the powdered salts are characteristic of non-crystalline materials (**Figure 2**), possibly due to the used isolation method (see **Section 2.1**). Na_2HFol exhibits a diffraction peak at $2\theta = 27.10°$ (*ca.* 0.33 nm) attributed to the distance among two disk-like structures π–stacked in a columnar array, formed by the self-assembly of $HFol^{2-}$ anions in water [25,27,53], as discussed in **Section 3** of **SM**. Hence, the only coherence length detected by XRD is the ordered structure arising from the periodicity of π–π intermolecular stacking [53]. On the other hand, XRD pattern of Na_3Folate presents only a broad peak centered around 2θ of 25°, indicating that the deprotonation of N(3)-H group precludes the formation of the disk-like tetramer arrays, and their stacking, probably because of the repulsive forces between negatively-charged PT units.

Samples present distinct colors (not shown): while powdered commercial FA is yellow orange, Na_2HFol is orange and Na_3Fol is yellow. The intermolecular interactions as H-bonds and π–π stacking modify the electronic and vibrational spectra of the molecular and anionic organic aggregates in comparison with their respective monomeric species [54,55]. To complement the XRD results, the UV-VIS diffuse reflectance spectra of FA and sodium salts were recorded. The electronic absorption spectra in the solid state (aggregated form) are compared with the spectra of compounds in aqueous solution (monomeric form), as displayed in **Figure 3**.

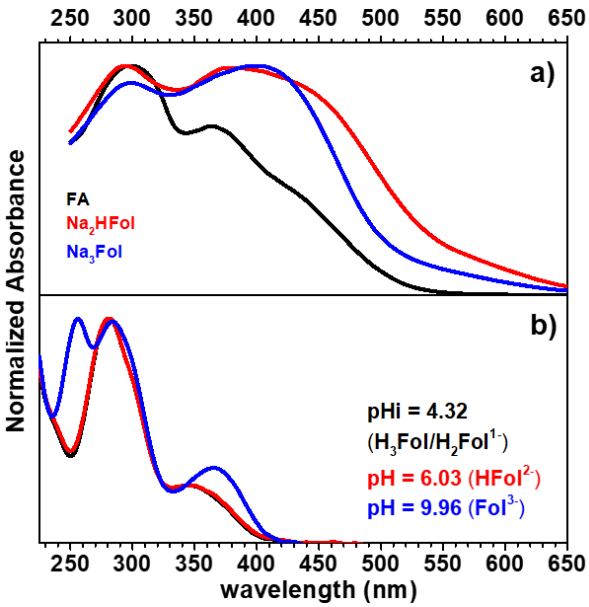

Figure 3. a) UV–VIS diffuse reflectance spectra of FA, Na_2HFol and Na_3Fol samples compared with b) electronic spectra of FA titrated in water; pHi is the initial pH value after FA dissolution in water.

Data about the electronic UV-VIS spectra of FA in solution are revisited and a discussion is reported in **Section 4** of **SM**. According to **Figure A.4**, only Fol^{3-} species can be distinguished in solution. However, a solution-to-solid spectral shift is clearly observed, and the powdered samples present distinguishable electronic spectra, what could indicate the different species and/or aggregated states.

UV-VIS electronic spectrum of commercial FA in solid state exhibits bands centered at 296 nm and 365 nm (**Figure 3**). The position of the higher-energy band is not affected by the deprotonation degree of the species, since it is also observed for Na_2HFol and Na_3Fol. Considering that the band around 280 nm in water solution is attributed to the π–π* transition of PT and *p*-ABA moieties in FA and Na_2HFol, and to the π–π* transition of *p*-ABA [34,56] in Na_3Fol sample, the same assignment seems plausible for the solid state samples. The band at about 365 nm is tentatively correlated to the band at 346 nm present in the spectra recorded in solution, which is attributed to

the π–π*/n–π* of PT ring [34,56]. The spectrum of FA in solid state presents additionally a shoulder in the 430 nm region that can be attributed to an intermolecular charge-transfer (CT) transition from the benzene to the pyrazine rings of aggregated molecules [29,57] because of their proximity in the crystal (**Figure A.2**).

The electronic spectrum of powdered Na_2HFol presents a very broad band in the region of 350-420 nm with an intense shoulder around 450-550 nm, that is not observed in water solution, as noticed to FA in solid state (**Figure 3**). As discussed previously, Na_2HFol assembles in a supramolecular structure, in which H-bonded folate tetramers are tightly packed in a π-stacking array (**Figure A.3**). Consequently, the spectral profile of the dianion salt in the 400-550 nm region could be attributed mainly to an CT transition favored by some intermolecular interactions, based on study of concentrated solution of FA [57] and nanoparticles of pyrazoline derivate [58]. On the other hand, Na_3Fol shows a distinct spectral profile, in which a broad band arising in the 400 nm region is more intense than that at 296 nm. The hyperchromic shift should be attributed to the deprotonation of PT ring, which changes the energy of π–π */n–π* transitions, as observed for Fol^{3-} in aqueous solution. Besides, a tail extended up to about 500 nm is observed in the solid state Na_3Fol spectrum, also suggesting a charge transfer transition, but less intense than for Na_2HFol.

The UV–VIS diffuse reflectance results are in line with the XRD data interpretation regarding the structural arrangement of FA and folate species in the samples and their aggregation degree; these techniques can be used to differentiate disodium and trisodium folate compounds.

3.2. Thermal Analysis (TG/DTG-DSC) coupled to mass spectrometry (MS)

The DSC curves in N_2 atmosphere and the data from melting point analysis (**Figure A.5**) of FA, Na_2HFol and Na_3Fol pointed out that the samples decompose at about 210 °C, 280°C and 300°C, respectively, as discussed in **Section 5** in **SM**.

The results of thermal analysis in air atmosphere are displayed in **Figure 4**, summarized in **Table 1**, and detailed reported in **Table A.1** of the **SM**. The first thermal event for all samples is attributed to the dehydration step (endothermic processes), as indicated by the release of the fragment *m/z* =18 (H_2O). Considering the beginning of the release of fragment attributed to CO_2 (*m/z* = 44 in MS curve; **Figure 4b**), the thermal stability of FA is significantly increased in salt forms: from 198 ºC (FA) to 267 ºC (Na_2HFol) and to 300 ºC (Na_3Fol), in line with reported data for some folate metal complexes [19,21] and alkaline salts [41]. The decomposition temperature values of FA and its salts are practically the same in inert (N_2; **Section 5** of the **SM**) or oxidant (**Figure 4**) atmospheres, which indicate a process driven by thermolysis [59].

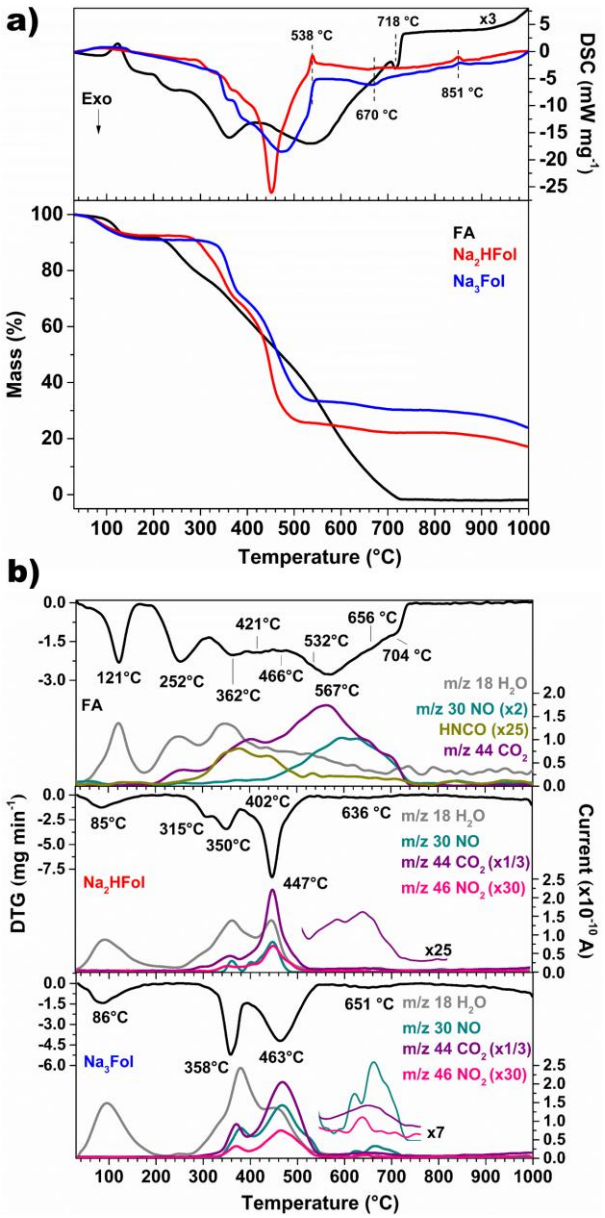

Figure 4. a) TG-DSC and b) DTG-MS curves of commercial FA, and synthesized Na_2HFol and Na_3Fol samples, under air atmosphere.

Table 1
Thermal analysis data of FA, Na_2HFol and Na_3Fol samples under air atmosphere.

Sample	H_2O (%)[a]	Organic matter (%)	Proposed Formula[b]
FA	7.9 (7.5)	93.8 (92.5)	$C_{19}H_{19}N_7O_6 \cdot 2.0H_2O$
Na_2HFol	7.6 (8.5)	81.5 (82.7)	$Na_2C_{19}H_{17}N_7O_6 \cdot 2.5H_2O$
Na_3Fol	9.0 (9.6)	76.7 (78.0)	$Na_3C_{19}H_{16}N_7O_6 \cdot 3.0H_2O$

[a]hydration water; [b]from thermal analysis results; Values in parenthesis are the expected percentage considering the proposed formulas.

As previously recorded by Vora et al. [60], crystalline FA presents a complex thermal decomposition mechanism in N_2 atmosphere. Indeed, it was also observed in air

atmosphere, as displayed in **Figure 4**, **Table A.1** and in **SM**. After dehydration, the TG curve of FA presents a slow weight loss profile. The oxidative decomposition of FA takes place in five consecutives events of mass loss, divided at least in nine overlapped steps (TG-DTG; **Table A.1**). The two overlapped events in 190-391°C range may be mainly attributed to the Glu moiety decomposition (calc. 27.7%; exp. 27.5%). The former event is accompanied by the release of H_2O and CO_2 (190-391 °C) as well as by the release of a fragment with *m/z* = 43, assigned to HNCO (292-391°C). In the region between 391-528 °C, the events can be mainly attributed to the oxidative decomposition of *p*-ABA group (calc. 25.4%; exp. 25.6%). The event is accompanied mainly by the release of H_2O, CO_2, and HNCO. Since the higher amounts of released *m/z* = 30 (NO) and *m/z* = 44 (CO_2) are observed between 528-707 °C, the event occurring in this temperature region is predominantly associated to the PT rings decomposition (calc. 39.4%; exp. 38.6%), which is the moiety with the highest nitrogen content.

A change in the thermal behavior of sodium folate salts is observed comparing with FA. The steps of the thermal oxidation of sodium salts are not easy to separate. Unlike FA, the TG curves of salts after dehydration present abrupt weight loss events (**Figure 4**). For Na_2HFol, the decomposition of anhydrous sample occurs mainly in three events (six steps). In the range of 264-323 °C, the event is accompanied by the release of H_2O and CO_2 and can be related to the decomposition of carbon chain (C_3H_4) of glutamate moiety (calc. 7.7%; exp. 7.8%). The following events are accompanied by the release of H_2O, CO_2, NO and fragment of *m/z* =46 (NO_2) and are related to the decomposition of *p*-ABA (323-528°C; two steps) and PT (383-528 °C) groups. Dehydrated Na_3Fol presents only two overlapped events attributed to folate decomposition. In the region between 292-394 °C, the event is associated to the decomposition of glutamate and the initial decomposition of *p*-ABA. It is accompanied

by the release of H_2O, CO_2, NO and NO_2. The next event (394-547 °C) is followed by the same gaseous product, and it may be mostly attributed to the final decomposition of *p*-ABA and PT.

The events of small weight loss for salts above 530 °C are associated to the release of different gaseous products (detected by MS, as detailed discussed in **Section 6** of **SM**). For Na_2HFol, the event is associated only to the release of CO_2, while for Na_3Fol, it is accompanied by the release of NO, NO_2 and CO_2. Residual mass at 800 °C are consistent with the formation of Na_2CO_3 residue: 22.6% (calc. 20.0%) for Na_2Hfol and 30.0% (calc. 28.3%) for Na_3Fol.

Regardless of the atmosphere (*i.e.*, air or N_2), the thermal stability ranks as Na_3Fol > Na_2HFol > FA. The sodium salts are an alternative to improve the thermal stability of FA, especially in the case of Na_3Fol salt with a gain of stability of about 100 ºC. Additionally, the thermal analysis results indicate that the decomposition of Glu seems to be delayed in the salts while the end of oxidative decomposition of PT ring appears to be advanced.

3.3. Structural simulation of FA, Na_2Fol and Na_3Fol by DFT

The conformations calculated for FA, Na_2HFol and Na_3Fol, using the B3LYP/6-311++G(d,p) gaussian basis sets in the DFT framework, are shown in **Figure 5**. The obtained structures (simulated in gas phase) exhibit essentially the same extended conformation for the three species, independently of the protonation level: a planar pteroic acid unit (PT and *p*-ABA structures), a *trans* amide bond and a bent conformation of the Glu moiety.

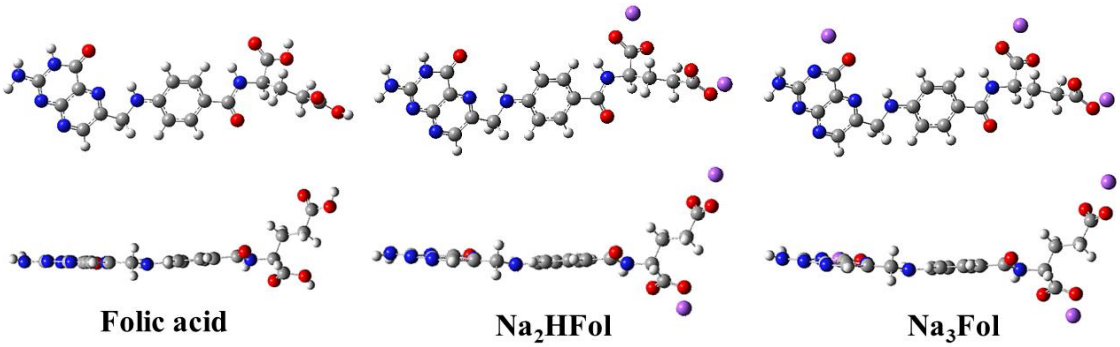

Figure 5. Theoretically (DFT) optimized structures (in vacuum) of FA, Na_2HFol and Na_3Fol. Color conventions: carbon (grey), hydrogen (white), oxygen (red), nitrogen (blue) and sodium (purple).

The DFT simulated FA structure achieved in this work was compared to the crystal structure of dihydrate FA resolved by the Rietveld refinement of powder X-ray diffraction data [52] (**Table A.2**). Kaduk et al. [52] performed geometry optimization *via* DFT (using the CRYSTAL09 software) and considering $C_{29}H_{29}N_2O_6(H_2O)_2$ in the unit cell of FA. The main differences between experimental and simulated data are: (*i*) the PT and *p*-ABA acid units are not co-planar (**Figure 5**); and (*ii*) the bent of Glu moiety is not in the same three-dimensional conformation. In addition, such conformational structure significantly contrast from that of FA and folate^{2-} predicted by molecular simulation in liquid solution [38,61], and of folate^{2-} complexed to enzymes, as for instance the dihydrofolate reductase (DHFR) [40] or the folate receptor alpha (FRα) [39].

A particularly good agreement between the calculated and experimental bond lengths and angles values is here obtained although the simulations considered the isolated molecule, *i.e.*, intermolecular interactions are disregarded. It is worth to note that the calculated C4=O bond distance of 1.211 Å is close to the experimental value of 1.208 ± 0.004 Å [52] and it evidences the keto form PT moiety in FA. To the best of our

knowledge, the crystal structure of dianion or trianion folate salts has not been reported so far, precluding any possible comparison.

Comparing the DFT results for FA in relation to Na_2HFol (**Table A.2**), the main modifications are: *(i)* the length of C–O bonds of both carboxylic groups, indicating their deprotonation; *(ii)* the elongation of Cα–Cα' and Cγ–Cγ' bonds; and *(iii)* the decreasing of Cα–Cα'–Oα' and Cγ–Cγ'–Oγ angles. According to theoretical calculations (and as expected), deprotonation of FA into the dianion promotes changes in the glutamic unit while the pteroic acid moiety is insensitive. On the other hand, comparing the structural parameters calculated for Na_2HFol and Na_3Fol (**Table A.2**), the main differences are: *(i)* the C4–O distance increases from 1.211 Å in the simulated FA and Na_2HFol to 1.258 Å in Na_3Fol, thus indicating that the bond order decreases and that the enolate turns to be the predominant mesomer form (**Figure A.1**).

In the pyrimidine ring, the C4–N3 and C2–N3 lengths decrease, respectively, from 1.408 Å to 1.367 Å and from 1.377 Å to 1.357 Å. The N3–C4–C4a and N1–C2–N3 angles increase while the O–C4–C4a and C2–N3–C4 angles are reduced. Although there are no experimental data to compare with the DFT in the case of Na_3Fol, the experimental crystallographic results obtained for PT anion coordinated to rhenium(I) [20] by O4 and N5 atoms show similar modifications (**Table A.2**). In the metal complex, the deprotonation of N3 promotes the shortening of C4–N3 (1.326(6) Å) and the elongation of the C4–O (1.283(5) Å), characteristic of enolate mesomer form [20].

3.3. IR and Raman vibrational spectroscopies

The experimental IR and Raman spectra of FA and sodium folate salts in the 1800-800 cm^{-1} region are presented in **Figure 6**. Outside this spectral range, the information is limited; the bands in the region of 4000 and 2900 cm^{-1} are associated to

the stretching modes of OH, NH, CH and CH_2 groups [62]. **Figures A.6-A.8** (full experimental spectra) show a strong band broadening in folate salts spectra, mainly due to intermolecular hydrogen bonds interactions between water molecules and/or folate anions groups such as -NH, >C=O and $-COO^-$ [62]. The region below 800 cm^{-1} shows very weak bands similar for all samples.

As highlighted in gray in **Figure 6**, experimental IR and Raman spectra of FA, Na_2HFol and Na_3Fol show distinct profiles. The detailed assignment of FA and folates bands is not straightforward due to the structural complexity of the molecule/anions and because many vibrational modes are combined. Hence, a tentative attribution of vibration modes presented in **Table 2** is proposed considering the changes observed according to the protonation degree of the compound, in the light of DFT calculations for the species in vacuum, as well as from data in the literature [30,33,41–44, 62–74]. The comparison between experimental and theoretical spectra is shown in **Figures A.9-A.11**. As displayed in **Figure A.12**, a good linear correlation ($R^2 > 0.998$) is observed between the experimental and calculated energy (in wavenumber). In the following, the main distinct regions of vibrational spectra of FA, Na_2HFol and Na_3Fol are discussed while some less relevant bands are considered in **SM** (**Figures A.9-A.11**).

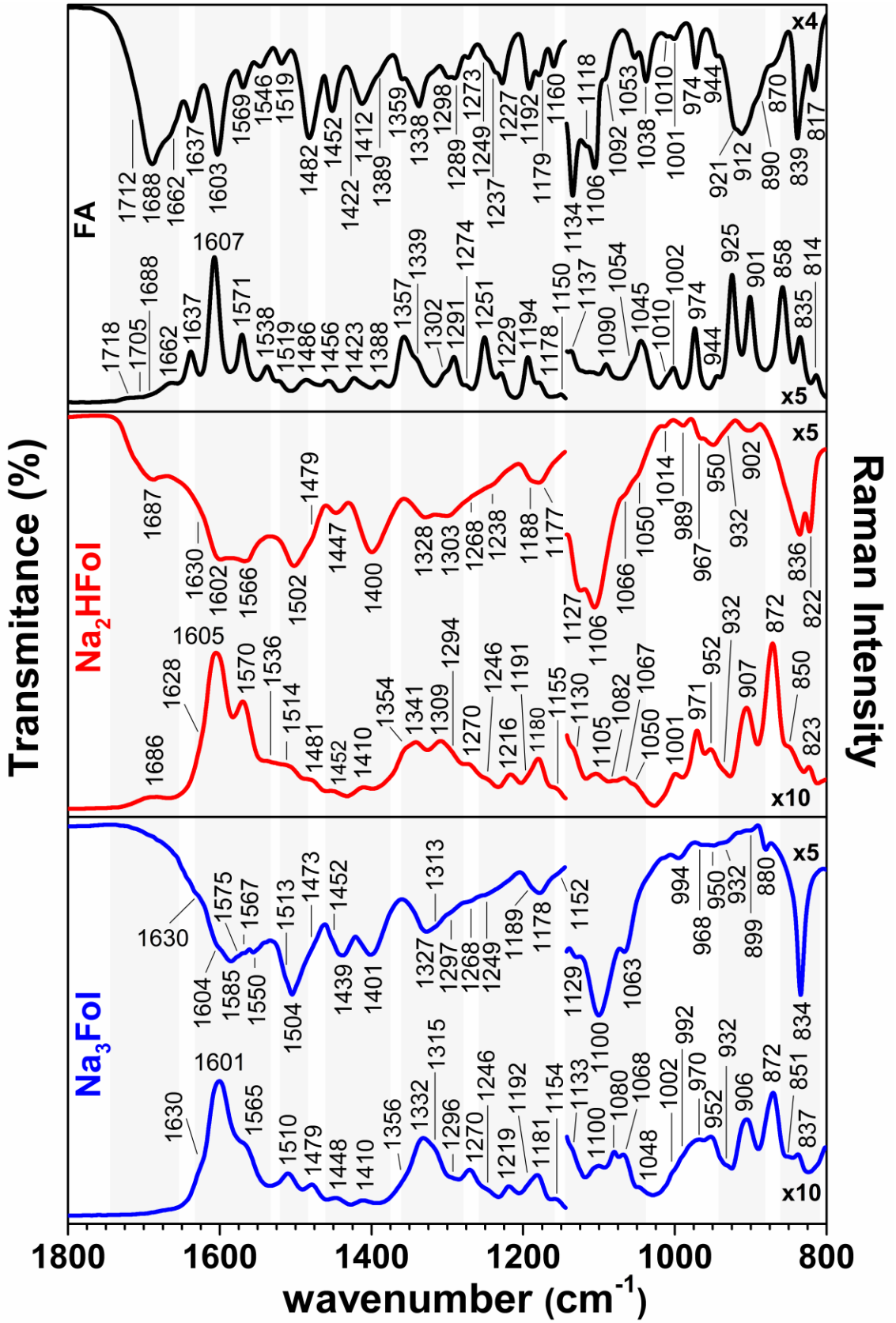

Figure 6. Experimental infrared (top) and Raman (down) spectra of FA, Na_2HFol and Na_3Fol samples.

Table 2. Experimental and calculated IR and Raman wavenumber values (cm^{-1}) for FA, Na_2HFol and Na_3Fol

Folic Acid			Na_2HFol			Na_3Fol			Tentative attribution of main groups involved in the vibration[b,c,d,e]
calc.[a]	exp.		calc.[a]	exp.		calc.[a]	exp.		
	IR	Raman			Raman		IR	Raman	
1766	1712 sh	1718 w							ν(Cγ'=O)
1758		1705 w							ν(Cα'=O)
1737	1688	1688 sh	1737	1687	1686				ν(C4=O) + δ(N3H) + sc(NH_2)
1656	1662 sh	1662	1654	1630 sh	1628 sh	1652	1630 sh	1630 sh	ν(C11=O) + δ(N12H) + ϕ[*8b*]/D23
1634	1637	1637	1634						νas(N2C2N1) + sc(NH_2) + δ(N3H)
1607	1603	1607	1608	1602	1605	1609	1604 sh	1601	ϕ[*8a*]/D3
						1598	1585	#	sc(NH_2) + ν(PT rings) + ν(C4–O^-)
						1577	1575 sh	#	ν(PT rings) + sc(NH_2) + ν(C4–O^-)
1563	1569	1571	1565	1566	1570				ν(PT rings) + sc(NH_2) + δ(N3H); ϕ[*8b*]/D23 + δ(N10H) + ν(C11=O)
						1562	1567	1565 sh	ϕ[*8b*]/D23 + δ(N10H) + ν(C11=O)
						1544	1550 br	#	ν(C4–O^-) + ν(PT rings) + sc(NH_2)
			1543	#	#	1541			νas(Cα'OO^-) + ν(C11N12)/δ(N12H)
1530	1546	1538	1528	#	1536 sh				ν(PT rings) + δ(N3H) + ν(C4=O); ϕ[*19a*]/D4 + ν(N10-ϕ)/δ(N10H) + ν(C11-ϕ) + δ(N12H)
1524	1519	1519 sh	1519	#	1514 sh				ϕ[*19a*]/D4 + ν(N10-ϕ)/δ(N10H) + ν(C11-ϕ) + ν(C11N12)/δ(N12H); ν(PT rings) + δ(N3H)
						1518	1513 sh	1510	ν(PT rings) + sc(NH_2) + ν(C4–O^-); ϕ[*19a*]/D4 + ν(N10-ϕ)/δ(N10H) + ν(C11-ϕ) + ν(C11N12)/δ(N12H);
			1515	1502 br		1514	1504 br		νas(Cγ'OO^-)
1480	1482		1475	1479 sh					ν(C11N12)/δ(N12H); sc(C$βH_2$); ν(PT rings) + δ(N3H) + sc($C9H_2$); ϕ
						1468	1473 sh		ν(C11N12)/δ(N12H); sc(C$βH_2$); sc($C9H_2$) + ν(PT rings); ϕ
1465	1452	1456	1460	1447	1452				sc($C9H_2$) + ν(PT ring); sc(C$βH_2$)/(C$γH_2$); ν(C11N12)/δ(N12H); ϕ
						1459	1452 sh	1448 br	sc(C$βH_2$)/(C$γH_2$); ν(C11N12)/δ(N12H)
						1423	1439		ν(PT rings) + ν(C2N2)
1412	1412	#	1407	#	1410	1408	#	1410	ϕ[19b]/D4; ω($C9H_2$)
			1396	1400 br		1396	1401 br		νs(Cα'OO^-)/ν(Cα-Cα') + ω(C$βH_2$)/(C$γH_2$);
			1386			1386			νs(Cγ'OO^-)/ν(Cγ-Cγ') + ω(CγH2)
1385	1389 sh	1388							δ(OH) + ω(C$βH_2$)/(C$γH_2$)
1365	1359								δ(OH) + δ(CαH) + ω(C$γH_2$)/τ(C$βH_2$) + ν(C11N12)/δ(N12H); ω($C9H_2$) + δ(N10H)/ν(N10-ϕ) + ϕ; ν(PT rings) + δ(N3H) + δ(C7H)
						1355	#	1356 sh	ω($C9H_2$) + δ(N10H)/ν(N10-ϕ) + ϕ
						1346			ν(PT rings) + ν(C2N2) + δ(C7H)

Table 2. *Continued…*

Folic Acid			Na_2HFol			Na_3Fol			Tentative attribution of main groups involved in the vibration[b,c,d,e]
calc.[a]	experimental		calc.[a]	Experimental		calc.[a]	experimental		
	IR	Raman		IR	Raman		IR	Raman	
1346		1357	1344		1354 sh				ν(PT rings) + $\tau(NH_2)$ + δ(C7H) + $\omega(C9H_2)$
			1336	1328 br		1336	1327 br		$\omega(C\beta H_2)/(C\gamma H_2)$ + $\delta(C\alpha H)$ + $\nu s(C\alpha'OO^-)$
1333	1338	#							δ(OH) + $\delta(C\alpha H)$ + $\tau(C\beta H_2)/\omega(C\gamma H_2)$
1326									ϕ[14]/D25 + ν(N10-ϕ) + $\omega(C9H_2)$; $\tau(C\beta H_2)/(C\gamma H_2)$ + $\delta(\alpha'OH)$ + $\delta(C\alpha H)$
1323	#	1339	1323	#	1341				ν(PT rings) + δ(N3H) + $\tau(NH_2)$ + δ(C7H) + $\omega(C9H_2)$ + ν(N10-ϕ) + [*14*]/D25
			1318	1328 br	#				ϕ[*14*]/D25 + ν(N10-ϕ) + $\omega(C9H_2)$ + ν(PT rings) + δ(N3H); $\omega(C\beta H_2)/\tau(C\gamma H_2)$ + $\delta(C\alpha H)$
						1320	1327 br	#	ϕ[*14*]/D25 + δ(N10H)/ν(N10-ϕ); $\omega(C\beta H_2)/(C\gamma H_2)$ + $\delta(C\alpha H)$
						1308	#	1332	ν(PT rings) + $\tau(NH_2)$ + δ(C7H) + $\omega(C9H_2)$ + δ(N10H)/ν(N10-ϕ) + ϕ
						1301	1313 sh	1315 sh	ν(PT rings) + ν(C2N2) + δ(C7H) + $\omega(C9H_2)$; δ(OH) + $\tau(C\beta H_2)/(C\gamma H_2)$ + $\delta(C\alpha H)$; ϕ[*3*]/D26; ν(PT rings) + δ(N3H) + ν(C2N2);
1304	1298	1302 sh							
			1300	1303	1309				ϕ[*3*]/D26 + ν(C11N12)/δ(N12H) + $\delta(C\alpha H)$ + $\tau(C\beta H_2)/(C\gamma H_2)$; ν(PT rings) + ν(C2N2) + δ(N3H);
						1299	1297 sh	1296 sh	ϕ[*3*]/D26 + ν(C11N12)/δ(N12H) + $\delta(C\alpha H)$ + $\tau(C\beta H_2)/(C\gamma H_2)$
1293	1289	1291							δ(OH) + τ(CβH2)/(CγH2) + $\delta(C\alpha H)$ + ν(C11N12)/δ(N12H)
1286			1285	#	1294 sh				ν(PT rings) + δ(N3H) + ν(C2N2) + δ(C7H) + $\omega(C9H_2)$ + δ(N10H); ϕ
1114	1106	#							$\nu(C{-}O)_{OH}$ + $\omega(C\beta H_2)/(C\gamma H_2)$
1104			1104	1106	1105				ϕ[18b]/D24 + ν(C9N10) + ν(PT rings) + δ(N3H) + $\rho(NH_2)$
						1101	1100	1100	ϕ[18b]/D24 + ν(C9N10) + ν(PT rings)
			842*	836	#	841*	834	837	ϕ[*17b*]/D16 + δoop(C11N12H) + δoop(N10H);
838*	839	835							ϕ[*17b*]/D16 + δoop(C11N12H) + δoop(N10H); ϕ[*18a*]/D10 + $\nu(Glu)_{ch}$ + δoop(COOH)
						832*	834	837	δoop(PT rings) + $\rho(C9H_2)$
815*	817	814							δoop(PT rings) + $\rho(C9H_2)$; ϕ[*10a*]/D13
			816*	822	823				δoop(PT rings) + $\rho(C9H_2)$; ϕ[*10a*]/D13; $\tau(C\gamma H_2)/(C\beta H_2)$ + δoop(COO^-)
652	912(br)								δoop(γ'OH)
596									δoop(α'OH)

(a) Selected values in wavenumbers (cm^{-1}) obtained using the functional/basis set B3LYP/6-311++G(d,p). Wavenumbers were multiplied by the 0.975 scaling factor (* indicates unscaled values); # are very weak and/or not resolved band; (b) Attributions were made in the light of DFT and works from the literature [30,33,41–44,62–74]; (c) νs = symmetric stretching, νas = antisymmetric stretching, δ = bending (in plane; ip); oop = out-of-plane, sc = scissoring (ip bending), ω = wagging (oop bending), ρ = rocking (ip bending), τ = twisting (oop bending), b = broad, sh = should, w = weak, $(GLU)_{ch}$ = carbonic chain of Glu /glutamate; (d) The numbers and letters are related to the carbon indexation in FA structure shown in Figure 1a; (e) phenylene ring (ϕ) vibration modes were assigned using Wilson and Mulliken labelling [73];

1720-1630 cm^{-1} range. This region is assigned mainly to the bands related to the Cα'=O and Cγ'=O stretching (ν) vibrational modes of Glu unit, C4=O of PT ring and C11=O of amide group. Compared to the FA vibrational spectra obtained by DFT (vacuum simulation), the experimental bands are not as well resolved and are shifted to lower energy range (**Figure A.9**). It can be associated to the network of intermolecular hydrogen bonds in the solid (**Figure A.2**), which makes the C=O bond weaker, leading to a red shift and a broadening of the related bands [62]. The three compounds possess hydration water, as observed in thermal analysis data, which bands observed around 1650-1620 cm^{-1} in the infrared spectra are assigned to angular deformation [62].

The ν(C=O) vibrational modes of Glu moiety, attributed to the carboxylic groups identified as α' and γ' in **Figure 1**, are predicted by DFT to be coupled. However, as noticed in **Figure A.13**, the energy of ν(Cγ=O) vibration is higher than that of ν(Cα=O), as expected considering that the first bonging is shorter than the second one (**Table A.2**). Experimentally, it is observed as a shoulder at around 1712 cm^{-1} in the infrared and as weak bands in the FA Raman spectrum, in agreement with Braga et al. [41] These bands are not present in the spectra of the sodium salts indicating the deprotonation of Glu moiety.

A band assigned to C4=O stretching of PT ring is observed at around 1688 cm^{-1}, both in FA and Na_2HFol experimental infrared spectra, though less intense in the last compound. The band position is in agreement with the value for guanine (pyrimidine ring fused to imidazole) at 1697 cm^{-1} [69]. This band is absent in the Na_3Fol spectrum, indicating the deprotonation of N3 atom of PT and the formation of the enolate group (**Figure A.1**).

For the three species, the ν(C11=O) of amide (Amide I) is predicted by DFT at 1650 cm^{-1} region. The experimental band is observed at 1662 cm^{-1} as a shoulder in

infrared and a weak band in Raman spectra of FA, in line with results reported for peptides (peptide bonds) [65]. However, it is proposed here that this band is red shifted to 1630 cm^{-1} due to intramolecular hydrogen bonds between N12–H and γ'COO^- groups, as suggested by Gocheva et al. [38] for Fol^{2-} in aqueous solution and by similar values observed for polypeptides [65].

According to DFT, in the FA spectrum, the band at 1637 cm^{-1} (calc. 1634 cm^{-1}) can be attributed to antisymmetric stretching (νas) of guanidyl group (C2 bonded to N1, N2 and N3; $C2N_3$), coupled to NH_2 scissoring (sc) and N3–H bending (δ), as presented in **Figure A.14**.

1610-1520 cm^{-1} range. Regardless of the sample, a strong band at about 1600 cm^{-1} is observed in the infrared and Raman spectra (**Figure 6**), indicating a vibration from a group not involved in the deprotonation process. Based on DFT and in agreement with Kokaislová et al. [30] and Braga et al. [41], it is assigned to the C-C stretching of phenylene ring of *p*-ABA group. For FA and Na_2HFol, the bands in the 1570 cm^{-1} region of infrared and Raman spectra are attributed to vibrations from pteroic acid unit (**Table 2**), consistent with experimental and theoretical results reported for guanine [64,69], *p*-ABA [71], PT [70], and FA [41]. A broadening of bands is observed from FA to Na_2HFol, possibly due to the H-bonds and π–π interactions, as discussed previously.

Comparing the spectra of Na_2HFol and Na_3Fol, notable changes in the spectral profile are observed. According to DFT calculations, such changes are attributed to the deprotonation of N3–H group, which promotes a redshift ($\Delta\nu$ = 36 cm^{-1}) of the band assigned to PT vibrational modes from 1634 cm^{-1} (in FA; previously discussed) to 1598 cm^{-1} in theoretical spectra (**Table 2** and **Figure A.14**). As theoretically predicted by Reibnegger [50] the N3–H deprotonation leads to the improvement of aromatic character of pyrimidine ring in anionic pterin. Considering that fused aromatic rings

have almost the same vibrational energy as benzene derivatives [62], the shift of the band toward C-C stretching phenylene rings is in line with theoretical calculation [50] and with the statement of enolate mesomer form in Fol^{3-} (**Figure A.1**).

DFT calculations indicate a pronounced band redshift ($\Delta\nu$ = 193 cm^{-1}) from 1737 cm^{-1} to 1544 cm^{-1} of ν(C4=O) due to the formation of C4–O^- (enolate, Fol^{3-}), as noticed in **Table 2** and **Figure A.15**. Theoretical and experimental vibrational studies performed with uracil (pyrimidine-2,4(1H,3H)-dione) also indicated a similar band shift [72]. In addition, band at around 1550 cm^{-1} for Na_3Fol has also the contribution of ν_{as}(Cα'OO^-) and ν(C11N12)/δ(N12–H) vibrations.

1520-1460 cm^{-1} range. The infrared spectra of folate salts show a strong and broad band at about 1500 cm^{-1} attributed to the νas(Cγ'OO^-). The broadening is probably due to some interactions by hydrogen bonds in the salts. DFT calculations indicate that the frequencies of the band of carboxylate groups are distinct for both folates: around 1543 cm^{-1} for ν_{as}(Cα'OO^-) and 1515 cm^{-1} for ν_{as}(Cγ'OO^-), as displayed in **Figure A.12**. Li et al. [67] observed the same result applying a DFT approach to disodium salt of folinate (both folinic and folic acids have a Glu and *p*-ABA groups) and suggested that the proximity of Cα'OO^- and N12–H groups can be the main reason for this frequency to be higher compared to Cγ'OO^- group.

The band at 1504 cm^{-1} is the most intense in the experimental infrared spectra of Na_3Fol (**Figure A.8**), while for Na_2HFol, the intensity of the bands at 1502 cm^{-1} and 1600 cm^{-1} is similar. Hence, Fol^{2-} and Fol^{3-} species can be discriminated by infrared spectroscopy merely by the analysis of the relative intensities of such bands. This change in the relative intensities can be attributed to the contribution of the band assigned mainly to ν(PT rings) and ν(C4–O^-), as can be noticed by the shoulder at 1513 cm^{-1} in the Na_3Fol experimental spectra (**Figure 6** and **Table 2**). According to DFT

calculations, such band is redshifted from 1530 cm^{-1} in FA to 1518 cm^{-1} in Na_3Fol theoretical spectra (**Table 2**). As seen in **Figure A.15**, the deprotonation of N3 increases PT stretching vectors, thus as well increasing the aromaticity of PT ring in Na_3Fol.

1460-1380 cm^{-1} range. All samples present two mainly bands around 1450 cm^{-1} and 1410 cm^{-1} in experimental infrared spectra. As the profile and relative intensity of these two main bands change according to the species (**Figure 6**), helpful to differentiate FA from folate salts. For FA and Na_2Hfol, the bands centered at around 1450 cm^{-1} (calc. around 1460 cm^{-1}) can be assigned to CH_2 and NH bending modes with contribution of PT rings stretching (**Table 2** and **Figure A.16**). The broad band around 1412 cm^{-1} in experimental infrared spectra of FA is assigned to CH_2 vibrations with contribution of in-plane δ(OH).

The broad and intense band observed at about 1400 cm^{-1}, in both infrared spectra of folate salts, can be mainly attributed to νs(COO^-), as listed in **Table 2**. For Na_3Fol, the band around 1450 cm^{-1} is observed as a shoulder in experimental spectrum and the contribution of PT vibration is no longer predicted by DFT (**Figure A.16**). Differently from Na_2HFol, a band centered at 1439 cm^{-1} is observed in experimental spectrum of Na_3Fol and with almost the same intensity as the above-mentioned band at 1400 cm^{-1}. Based on DFT calculations, it is correlated to the band at 1423 cm^{-1}, observed only in the simulated spectrum of Na_3Fol (**Figure A.9-A.11**) and attributed mainly to ν(PT rings), as displayed in **Table 2** and **Figure A.16**.

1360-1280 cm^{-1} region. Infrared and Raman spectra of FA present mainly four bands in this spectral range: two overlapped at about 1360-1340 cm^{-1} region and other two at 1300-1290 cm^{-1}. As proposed in **Table 2**, based on DFT, such bands are mainly associated to OH, CH and CH_2 bending of Glu unity and CC/CN stretching of aromatic

rings. Comparing FA and Na_2HFol spectra, modifications in the IR spectral profile are observed while the position of the bands is not changed significantly in Raman.

Based on DFT calculation and experimental results (**Figure 6** and **Table 2**), it is proposed that the bands at 1359 and 1338 cm^{-1} in IR spectra of FA are not from the same vibration of those respectively observed at 1357 and 1339 cm^{-1} in Raman. The change observed in IR spectra from FA to folate salts, is mainly due to Glu deprotonation. Bands attributed to CH and CH_2 bending of Glu moiety are shifted from 1338 cm^{-1} in FA to 1328/1327 cm^{-1} in folate salts. On the other hand, from Na_2HFol to Na_3Fol, both Raman and infrared spectra present significant modifications in this region. The infrared spectrum of Na_2HFol shows two bands centered at 1328 and 1303 cm^{-1} while Na_3Fol presents a broad band only at 1327 cm^{-1} (with a shoulder in 1313 cm^{-1}). In the Raman spectra, two resolved bands at 1341 cm^{-1} and 1309 cm^{-1} are observed for Na_2HFol, while for Na_3Fol such bands are overlapped and centered at 1332 cm^{-1} (with a shoulder at 1315 cm^{-1}). The bands in this spectral region are related to the C-C/C-N stretching and N3–H deformation mode, the last being absent in the trisodium.

According to DFT, after deprotonation of PT group, the C-C/C-N stretching is red shift from 1523 to 1508 cm^{-1} as well as blue shift from 1286 to 1301 cm^{-1}, both with a $\Delta\nu$ value of about 15 cm^{-1}, as displayed in **Figure A.17**. The observations are consistent with theoretical and experimental results (but in a minor shift extension) reported to uracil, which present such spectral features when its neutral pyrimidine ring is deprotonated in water [72]. The spectral profile in this region differentiates the dianionic from the trianionic folate. The resolution of the bands is higher in Raman than in infrared spectra. In addition, the shift observed for bands related to C-C/C-N stretching of PT unity after deprotonation occurs in a region around 1330 cm^{-1} attributed to C-C stretching of phenylene ring (**Table 2**). The results once again suggest an

improvement of aromaticity of PT ring and of the enolate mesomer form (**Figure A.1**) in Na_3Fol.

The observed difference of 15-20 cm^{-1} between theoretical and experimental results attribution of bands around 1360-1300 cm^{-1} in the Raman spectra (**Table 2**) is related to π–π interaction of aromatic rings between species. As discussed in the UV-VIS spectra and XRD data analysis, such interactions change the vibronic band structure [55] which is not taking into account in DFT calculations of single molecule in vacuum. In fact, a set of broad bands and shoulder overlapped in this region is observed in the Raman spectrum of Na_2HFol.

1100 cm^{-1} range. The band in the 1100 cm^{-1} region of FA and folates can be attributed mainly to in-plane C–H bending of phenylene ring coupled to C9–N10, in agreement to studies with tyrosine/tyrosinate [63] and as expected for amine linkage [62]. Vibrations attributed to ν(C–OH) of carboxylic groups and ν(PT rings) also have contribution in this region (**Table 2** and **Section 8** of **SM**). The striking changes from FA to Na_2Hfol are attributed to the deprotonation of Glu and the spectral changes from Na_2HFol to Na_3Fol are attributed to the deprotonation of N3–H. The band at 1100 cm^{-1} could be pointed as a marker of deprotonation degree since its relative intensity compared with other bands around 1130 cm^{-1} and 840 cm^{-1} regions change according to the species.

950-800 cm^{-1} region. Calculated DFT fits better with experimental spectra if the correction factor is not applied. This spectral range presents weak bands concerning out-of-plane δ(COO^-) and δ(COOH) vibrations. The most remarkable change in infrared spectra from FA to folate salts is the disappearance of the band in the region of 912 cm^{-1} attributed to out-of-plane δ(OH) group. DFT prediction for such vibration is not accurate if H-bonds are not considered [68]. For calculations of single molecule, the

band is predicted to be located in the region of 600 cm^{-1}, while for dimers it is predicted and experimentally observed at 960-900 cm^{-1} region, as in the case of dimers of benzoic acid [68] and mefenamic acid [43]. In this work, the calculated values are 652 cm^{-1} (γ'OH) and 596 cm^{-1} (α'OH) in agreement with the calculated values for benzoic acid [68]. The spectra of folate samples show bands at about 910 and 830 cm^{-1} assigned to the C-COO^- stretching, as observed for coumarate [42], pravastatin [44], or tyrosinate [74], for instance. As predicted by DFT calculations, the distance of Cα-Cα' or Cγ-Cγ' increases about 0.016 Å when FA is deprotonated (**Table A.1**), indicating that the chemical bond is weakened.

Another important change observed in IR spectrum of FA and folates occurs in the region of 840-816 cm^{-1}. FA and Na_2HFol present two bands in this region: (*i*) one at 839-836 cm^{-1} attributed mainly to out-of-plane C–H deformation of phenylene ring of *p*-ABA [63] and (*ii*) the other one at around 817-822 cm^{-1} attributed mainly to out-of-plane deformation of C-C/C-N and out-of-plane C–H deformation [63] from PT and *p*-ABA moieties, respectively. Otherwise, only one band at 834 cm-1 is observed for Na_3Fol. According to DFT calculations, the deprotonation of PT unit leads to a blue shift (Δν about 15 cm^{-1}) of C-C/C-N bending from 815 cm^{-1} to 832 cm^{-1} (**Figure A.18**).

3.5. Solid state ^{13}C-NMR spectroscopy

To the best of our knowledge, the ^{13}C-NMR data of di- and trianion folate species in solid state are not yet reported in the literature. Solid state ^{13}C and ^{15}N CP-MAS NMR of FA were reported by Ghosh, Gayen, and Dey [75]. Experimental results reported for FA in deuterated DMSO by Bonechi et al. [61] indicated that the molecular conformation is different from that observed in the crystal because intermolecular interactions in solution are not as important as in the crystal due to the intramolecular

interactions involving the Glu group. Experimental and simulated ^{13}C-NMR results for Fol^{2-} in water and for FA in DMSO were reported by Gocheva et al.[38] The authors also noticed the distinct conformation of FA in solution, in relation to the crystal, and predict that the molecules shape in "U" or "V" conformation because of the bending of Glu with *p*-ABA as well as the *p*-ABA with PT moiety.

Solid state ^{13}C-NMR spectra of AF, Na_2HFol and Na_3Fol samples are displayed in **Figure 7**. The peak assignments, based on DFT calculations and from data in the literature [38,61,75,76], are presented in **Table 3**. The attribution of ^{13}C NMR spectra peaks does not fully agree with previous studies [38,61,75,76] when the chemical shifts are too close from each other (for instance, C2 and C8a) . The experimental and calculated ^{13}C-NMR spectra of samples are compared in **Figure A.19**. A good linear correlation ($R^2 > 0.994$) between experimental and the calculated ^{13}C chemical shift can be noticed in **Figure A.20**.

The deprotonation of both carboxylic groups has weak influence on the ^{13}C chemical shifts of Cα, Cβ, Cγ, Cα' and Cγ' (**Figure 7**; **Table 3**), consistently with what was observed by Gocheva et al. [38] in DMSO. In addition, based on the DFT calculations, after the deprotonation, the chemical shift of Cγ' is larger than for Cα' (**Figure 7**; **Table 3**). Experimentally, both contributions merge at an average chemical shift value significantly smaller than that theoretically predicted, but partially correlated (**Figure A.20**). Another important spectral change experimentally observed is the chemical shift of C11 (from 164.9 to around 168.5) and C1' (from 116.9 to around 120.0) related to the amide group after Glu deprotonation. Such chemical shifts are also in agreement with Gocheva et al.[38]. C11 is the carbonyl group that links *p*-ABA to Glu moiety and, like in C1', the chemical shift seems to be overestimated by calculation in the three organic forms. It can be related to hydrogen bonds between N12–H and

Cγ'OO^- groups in anionic species [38], as discussed previously. For both salts, the C1' and C11 relative peak intensities of the sodic salts are weaker than for FA. In addition, after deprotonation, C6' and C4a+C2' peaks are overlapped in the spectra. DFT calculations are in close agreement with the experimental results for the two salts. However, the width of the contribution merging C6', C4a and C2' is of more than 500 Hz (> 6 ppm), explained by the fact that the π–π interactions (**Figure A.3**) are not considered in the calculations.

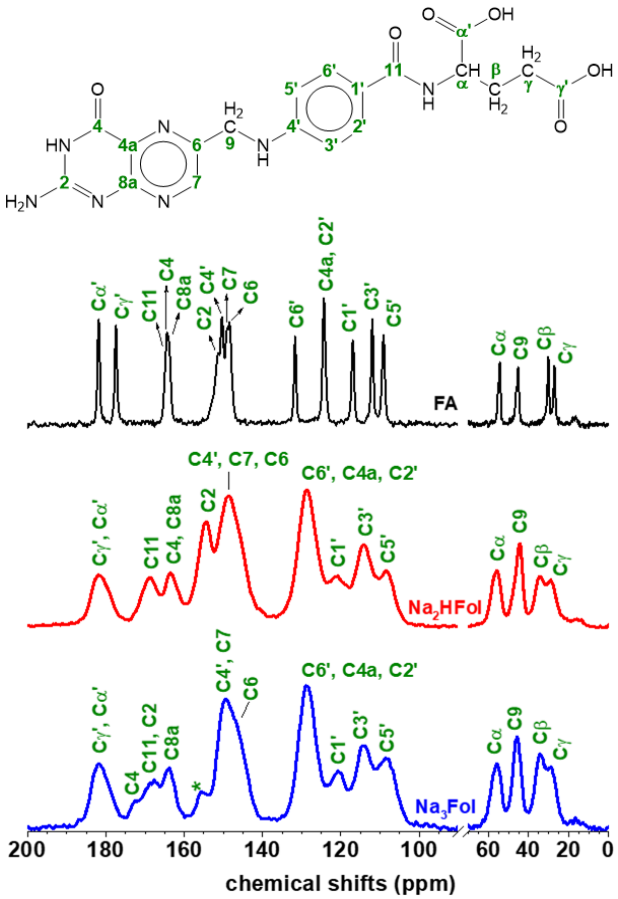

Figure 7. Experimental solid state ^{13}C-NMR spectra of commercial FA, and Na_2HFol and Na_3Fol samples prepared in this work. The peak marked with asterisk (*) indicates the possible presence of Na_2HFol.

The most remarkable chemical shift in the spectra of Na_3Fol compared with FA and Na_2HFol is associated to C4 and C2. Indeed, a pH superior to pK_{a4} induces a change from HN3 to NaN3 strongly impacting the neighboring carbon atoms, C2 and

C4, with a pronounced low-field shift. The results predicted by DFT are consistent with experimental chemical shift reported by Cheung et al. [76] for folate in water solution when the pH value is increased from 5.5 (Fol^{2-}) to 10 (Fol^{3-}). The same effect is predicted for DFT calculations but less pronounced for C4a and C8a (both engaged in the pyrazine resonant ring), but it is not experimentally observed because of the peaks broadening.

Table 3

Experimental and calculated solid state ^{13}C-NMR chemical shifts (ppm) of FA, Na_2HFol and Na_3Fol samples.

Assignment	Folic Acid					Na_2HFol				Na_3Fol		
	calcd.	exp.	exp.[a)]	exp.[b)]	exp.[c)]	calcd.	exp.	exp.[d)]	exp.[e)]	calcd.	exp.	exp.[f)]
α'C	180.4	181.8	182.1	173.7	173.7	191.4	181.8	182.0		191.6	181.8	
γ'C	178.4	177.4	186.4	173.9	173.9	192.1	181.8	185.1		192.1	181.8	
C11	168.5	164.9 sh	168.9	166.4	166.3	167.0	168.6	172.2		167.3	167.7	
C4	162.5	164.4	157.1	161.2	160.8	163.2	163.5	169.3	165.8	181.1	172.3	174.2
8a	161.7	164.0 sh	152.8	153.8	153.6	162.6	163.5	156.5	154.8	164.1	163.9	156.7
C2	154.2	151.2 sh	155.9	156.2	156.5	154.1	154.4	159.4	155.6	166.2	167.7	165.1
C4'	154.8	150.3	155.2	150.8	150.7	153.7	148.6	153.5		154.5	149.3	
C7	153.5	148.9 sh	153.2	148.6	148.6	153.6	148.6	151.4	150.1	152.8	149.3	148.5
C6	151.1	148.4	154.0	148.6	148.4	153.2	148.6	151.7	151.3	148.5	147.1 sh	148.9
C6'	137.5	131.6	136.4			137.0	128.7			137.1	127.7	
4a	133.4	124.3	128.9	127.9	127.8	133.1	128.7	130.2	128.5	131.5	128.7	129.2
C2'	130.8	124.3	136.4			131.0	128.7			130.7	128.7	
C1'	126.6	116.9	121.1	121.3	121.1	131.3	121.2	124.5		130.0	120.5	
C3'	116.5	111.9	116.5	111.2		116.1	114.2			115.6	114.2	
C5'	111.2	109.1	113.3	111.2	111.1	111.0	108.4	115.1		111.0	108.4	
αC	54.3	54.2	58.1	51.8	51.6	57.7	55.8	58.8		57.8	55.8	
C9	46.2	45.1	49.2	45.9	45.7	47.0	44.4	48.5	47.0	46.7	45.7	47.2
βC	33.5	30.1	30.8	26.1	25.9	37.5	34.3	31.4		37.6	34.3	
γC	31.6	27.1	33.9	30.4	30.3	37.3	29.1	37.1		37.2	28.9	

[a)]solid state ^{13}C CP-MAS NMR from ref. [75]; [b)] FA in DMSO-d6 solution from ref. [61]; [c)] FA in deuterated DMSO solution from ref. [38]; [d)]Fol^{2-} in water-d6 solution (pH 7) from ref. [38]; [e)]Fol^{2-} in deuterated water (pH 5.5) from ref. [76]; [f)]Fol^{3-} in deuterated water (pH 10) from ref. [76].

4. Conclusion

In this work, di- (Na_2HFol) and trisodium (Na_3Fol) folates isolated in their solid state are compared to FA, commercially available and applied in several fields. To highlight their respective characteristics, the three samples were characterized by spectroscopic (IR, Raman, and ^{13}C-NMR) and thermal techniques. The spectroscopic characterization, in combination with DFT theoretical calculations, allowed a complete spectral fingerprint of each compound. The main difference in the IR spectra between FA and Na_2HFol concerns the vibrational bands attributed to Glu /glutamate moiety while the most significant change between Na_2HFol and Na_3Fol is the absence of bands in the region of C=O stretching (1720-1660 cm^{-1}) and the relative intensity of bands at 1500 cm^{-1} and 1600 cm^{-1} (C-C stretching of the phenylene ring). Prominent modifications in the 1360-1290 cm^{-1} region of Raman spectra are associated to vibrational modes of PT rings.

Solid-state ^{13}C-NMR results show the successive deprotonation as a function of pH value. The carbon atoms of Glu moiety are not highly sensitive to the deprotonation while pronounced changes are related to chemical shifts of C1' (benzene ring) and C11 (amidic), from FA to Na_2HFol, and of C2 and C4 (PT moiety), from Na_2HFol to Na_3Fol.

Singular thermal oxidative profiles are observed for FA, Na_2HFol and Na_3Fol. Thermal stabilities of the samples are independent of the atmosphere (*i.e.*, air or N_2) and follows the order: Na_3Fol (300 ºC) > Na_2HFol (267 ºC) > FA (198 ºC). XRD pattern of Na_2HFol exhibits a broad diffraction peak that is attributed to the distance between two disk-like structures π–stacked in a columnar array, as already identified in water, thus underlining such organization in solid state.

UV-VIS electronic spectra of the species in water solution compared to those ones of the powdered samples are clearly distinguishable. In solid state, the spectra of all the three compounds show a shoulder in the low energy region, that can be associated to intermolecular charge-transfer (CT) transitions of packed FA molecules in the crystal, and, in the case of sodium salts, be related to CT transitions in aggregated and/or supramolecular structures.

It is our belief that this work provides comprehensive comparison between FA and its anionic folate species, helping to better understand and design new products based on them.

CRediT authorship contribution statement

V.R. Magri: Methodology, Investigation, Data curation, Writing - review & editing - original draft. **M.A. Rocha:** Methodology, Investigation, Data curation, Review. **C.S. de Matos:** Methodology, Investigation, Data curation, Review. **P.A.D. Petersen:** Theoretical calculations, Review. **F. Leroux:** NMR analysis, Review & editing. **H.M. Petrilli:** Theoretical calculations, Review & editing. **V.R.L. Constantino:** Conceptualization, Methodology, Visualization, Writing - review & editing, Supervision.

Declaration of Competing Interest

The authors declare that they have no known competing financial interests or personal relationships that could have appeared to influence the work reported in this paper.

Acknowledgments

V.R.M. is grateful to the Coordenação de Aperfeiçoamento de Pessoal de Nível Superior (CAPES, Finance Code 33002010191P0) for the PhD scholarship. C.S. de M. acknowledges the Fundação de Amparo à Pesquisa do Estado de São Paulo for research grant (FAPESP 2012/06291-4). V.R.L.C. and H.M.P. are thankful to the Conselho Nacional de Desenvolvimento Científico e Tecnológico (CNPq) for the research grants (305446/2017-7 and 311373/2018-6, respectively). This work is part of the Research Academic Cooperation Agreement PRC-CNRS-FAPESP (PRC-Projets de recherché conjoints 1688 and SPRINT-São Paulo Researchers in International Collaboration 2016/50317-9). The authors also acknowledge the Laboratório de Cristalografia (Instituto de Física - USP) for the XRD diffractograms registration and the Laboratório de Espectroscopia Molecular (LEM, Instituto de Química – USP) for the FTIR and Raman spectra recording.

Appendix A. Supplementary material

Supplementary data to this article can be found online at https://doi.org/XXX.

References

[1] R. Strouse, Folic Acid Market Size, Share & Trends Analysis Report by Application (Food & Beverages, Pharmaceuticals, Nutraceuticals), By Region, And Segment Forecasts, 2018 - 2025, Online. (n.d.) 135. https://www.grandviewresearch.com/industry-analysis/folic-acid-market.

[2] Z. Szakács, B. Noszál, Determination of dissociation constants of folic acid, methotrexate, and other photolabile pteridines by pressure-assisted capillary electrophoresis, Electrophoresis. 27 (2006) 3399–3409. https://doi.org/10.1002/elps.200600128.

[3] R.K. Saini, S.H. Nile, Y. Keum, Folates: Chemistry, analysis, occurrence, biofortification and bioavailability, Food Res. Int. 89 (2016) 1–13. https://doi.org/10.1016/j.foodres.2016.07.013.

[4] R.L. Blakley, IUPAC-IUB Joint Commission on Biochemical Nomenclature (JCBN). Nomenclature and symbols for folic acid and related compounds. Recommendations 1986, Eur. J. Biochem. 168 (1987) 251–253. https://doi.org/10.1111/j.1432-1033.1987.tb13413.x.

[5] J.L. Guéant, F. Namour, R.M. Guéant-Rodriguez, J.L. Daval, Folate and fetal programming: A play in epigenomics?, Trends Endocrinol. Metab. 24 (2013) 279–289. https://doi.org/10.1016/j.tem.2013.01.010.

[6] G.S. Ducker, J.D. Rabinowitz, One-Carbon Metabolism in Health and Disease, Cell Metab. 25 (2017) 27–42. https://doi.org/10.1016/j.cmet.2016.08.009.

[7] L. Qin, W. Wang, S. You, J. Dong, Y. Zhou, J. Wang, In vitro antioxidant activity and in vivo antifatigue effect of layered double hydroxide nanoparticles as delivery vehicles for folic acid, Int. J. Nanomedicine. 9 (2014) 5701. https://doi.org/10.2147/IJN.S74306.

[8] P. Jones, M. Lucock, C.J. Scarlett, M. Veysey, E.L. Beckett, Folate and Inflammation – links between folate and features of inflammatory conditions, J. Nutr. Intermed. Metab. 18 (2019) 100104. https://doi.org/10.1016/j.jnim.2019.100104.

[9] F. Ma, T. Wu, J. Zhao, A. Song, H. Liu, W. Xu, G. Huang, Folic acid supplementation improves cognitive function by reducing the levels of peripheral inflammatory cytokines in elderly Chinese subjects with MCI, Sci. Rep. 6 (2016) 1–11. https://doi.org/10.1038/srep37486.

[10] J.B. Wallingford, L.A. Niswander, G.M. Shaw, R.H. Finnell, The Continuing Challenge of Understanding, Preventing, and Treating Neural Tube Defects, Science (80). 339 (2013) 1222002–1222002. https://doi.org/10.1126/science.1222002.

[11] V. Kancherla, K. Wagh, Q. Johnson, G.P. Oakley, A 2017 global update on folic acid-preventable spina bifida and anencephaly, Birth Defects Res. 110 (2018) 1139–1147. https://doi.org/10.1002/bdr2.1366.

[12] M.A. Hofsäss, J. de Souza, N.M. Silva-Barcellos, K.R. Bellavinha, B. Abrahamsson, R. Cristofoletti, D.W. Groot, A. Parr, P. Langguth, J.E. Polli, V.P. Shah, T. Tajiri, M.U. Mehta, J.B. Dressman, Biowaiver Monographs for Immediate-Release Solid Oral Dosage Forms: Folic Acid, J. Pharm. Sci. 106 (2017) 3421–3430. https://doi.org/10.1016/j.xphs.2017.08.007.

[13] UNICEF Supply Division, Iron, folic acid and combined iron and folic acid tablets – technical bulletin, 2018. https://www.unicef.org/supply/documents/iron-folic-acid-and-combined-iron-and-folic-acid-tablets-technical-bulletin.

[14] C. Pagano, L. Perioli, L. Latterini, M. Nocchetti, M.R. Ceccarini, M. Marani, D. Ramella, M. Ricci, Folic acid-layered double hydroxides hybrids in skin formulations: Technological, photochemical and in vitro cytotoxicity on human keratinocytes and fibroblasts, Appl. Clay Sci. 168 (2019) 382–395. https://doi.org/10.1016/j.clay.2018.12.009.

[15] M. Scaranti, E. Cojocaru, S. Banerjee, U. Banerji, Exploiting the folate receptor α in oncology, Nat. Rev. Clin. Oncol. 17 (2020) 349–359. https://doi.org/10.1038/s41571-020-0339-5.

[16] B. Farran, R.C. Montenegro, P. Kasa, E. Pavitra, Y.S. Huh, Y.-K. Han, M.A. Kamal, G.P. Nagaraju, G.S. Rama Raju, Folate-conjugated nanovehicles: Strategies for cancer therapy, Mater. Sci. Eng. C. 107 (2020) 110341. https://doi.org/10.1016/j.msec.2019.110341.

[17] E. Nogueira, A.C. Gomes, A. Preto, A. Cavaco-Paulo, Folate-targeted nanoparticles for rheumatoid arthritis therapy, Nanomedicine Nanotechnology, Biol. Med. 12 (2016) 1113–1126. https://doi.org/10.1016/j.nano.2015.12.365.

[18] P.S. Kharkar, G. Soni, V. Rathod, S. Shetty, M.K. Gupta, K.S. Yadav, An outlook on procedures of conjugating folate to (co)polymers and drugs for effective cancer targeting, Drug Dev. Res. 81 (2020) 823–836. https://doi.org/10.1002/ddr.21698.

[19] M.G.A. El-Wahed, M.S. Refat, S.M. El-Megharbel, Synthesis, spectroscopic and thermal characterization of some transition metal complexes of folic acid, Spectrochim. Acta - Part A Mol. Biomol. Spectrosc. 70 (2008) 916–922. https://doi.org/10.1016/j.saa.2007.10.008.

[20] F. Ragone, G.T. Ruiz, O.E. Piro, G.A. Echeverría, F.M. Cabrerizo, G. Petroselli, R. Erra-Balsells, K. Hiraoka, F.S. García Einschlag, E. Wolcan, Water-Soluble (Pterin)rhenium(I) Complex: Synthesis, Structural Characterization, and Two Reversible Protonation-Deprotonation Behavior in Aqueous Solutions, Eur. J. Inorg. Chem. 2012 (2012) 4801–4810. https://doi.org/10.1002/ejic.201200681.

[21] P.R. Dametto, B. Ambrozini, F.J. Caires, V.P. Franzini, M. Ionashiro, Synthesis, characterization and thermal behaviour of solid-state compounds of folates with some bivalent transition metals ions, J. Therm. Anal. Calorim. 115 (2014) 161–166. https://doi.org/10.1007/s10973-013-3276-z.

[22] A.M. Naglah, M.S. Refat, M.A. Al-Omar, M.A. Bhat, H.M. Alkahtani, A.S. Al-Wasidi, Synthesis of a vanadyl (IV) folate complex for the treatment of diabetes: Spectroscopic, structural, and biological characterization, Drug Des. Devel. Ther. 13 (2019) 1409–1420. https://doi.org/10.2147/DDDT.S190310.

[23] A.A. El-Habeeb, Novel Gallium(III), Germanium(IV), and Hafnium(IV) Folate Complexes and Their Spectroscopic, Thermal Decomposition, Morphological, and Biological Characteristics, Bioinorg. Chem. Appl. 2020 (2020) 1–12. https://doi.org/10.1155/2020/6678688.

[24] C. He, M. Heidari Majd, F. Shiri, S. Shahraki, Palladium and platinum complexes of folic acid as new drug delivery systems for treatment of breast cancer cells, J. Mol. Struct. 1229 (2021) 129806. https://doi.org/10.1016/j.molstruc.2020.129806.

[25] S. Bonazzi, M.M. DeMorais, G. Gottarelli, P. Mariani, G.P. Spada, Self-Assembly and Liquid Crystal Formation of Folic Acid Salts, Angew. Chemie Int. Ed. English. 32 (1993) 248–250. https://doi.org/10.1002/anie.199302481.

[26] P. Xing, X. Chu, M. Ma, S. Li, A. Hao, Supramolecular gel from folic acid with multiple responsiveness, rapid self-recovery and orthogonal self-Assemblies, Phys. Chem. Chem. Phys. 16 (2014) 8346–8359. https://doi.org/10.1039/c4cp00367e.

[27] X. Wang, J. Sun, T. Li, Z. Song, D. Wu, B. Zhao, K. Xiang, W. Ai, X.Z. Fu, J.L. Luo, Folic acid self-assembly synthesis of ultrathin N-doped carbon nanosheets with single-atom metal catalysts, Energy Storage Mater. 36 (2021) 409–416. https://doi.org/10.1016/j.ensm.2021.01.024.

[28] H. Liu, Z. Li, Y. Sun, X. Geng, Y. Hu, H. Meng, J. Ge, L. Qu, Synthesis of Luminescent Carbon Dots with Ultrahigh Quantum Yield and Inherent Folate Receptor-Positive Cancer Cell Targetability, Sci. Rep. 8 (2018) 1086. https://doi.org/10.1038/s41598-018-19373-3.

[29] S. Gawęda, G. Stochel, K. Szaciłowski, Bioinspired nanodevice based on the folic acid/titanium dioxide system, Chem. - An Asian J. 2 (2007) 580–590. https://doi.org/10.1002/asia.200700025.

[30] A. Kokaislová, T. Helešicová, M. Ončák, P. Matějka, Spectroscopic studies of folic acid adsorbed on various metal substrates: does the type of substrate play an essential role in temperature dependence of spectral features?, J. Raman Spectrosc. 45 (2014) 750–757. https://doi.org/10.1002/jrs.4557.

[31] J.J. Castillo, T. Rindzevicius, K. Wu, C.E. Rozo, M.S. Schmidt, A. Boisen, Silver-capped silicon nanopillar platforms for adsorption studies of folic acid using surface enhanced Raman spectroscopy and density functional theory, J. Raman Spectrosc. 46 (2015) 1087–1094. https://doi.org/10.1002/jrs.4734.

[32] J.J. Castillo, T. Rindzevicius, C.E. Rozo, A. Boisen, Adsorption and Vibrational Study of Folic Acid on Gold Nanopillar Structures Using Surface-Enhanced Raman Scattering Spectroscopy, Nanomater. Nanotechnol. 5 (2015) 29. https://doi.org/10.5772/61606.

[33] R.A.R. Teixeira, F.R.A. Lima, P.C. Silva, L.A.S. Costa, A.C. Sant'Ana, Tracking chemical interactions of folic acid on gold surface by SERS spectroscopy, Spectrochim. Acta Part A Mol. Biomol. Spectrosc. 223 (2019) 117305. https://doi.org/10.1016/j.saa.2019.117305.

[34] M. Baibarac, I. Smaranda, A. Nila, C. Serbschi, Optical properties of folic acid in phosphate buffer solutions: the influence of pH and UV irradiation on the UV-VIS absorption spectra and photoluminescence, Sci. Rep. 9 (2019) 14278. https://doi.org/10.1038/s41598-019-50721-z.

[35] A.M. Abramova, A.A. Kokorina, O.A. Sindeeva, F. Jolibois, P. Puech, G.B. Sukhorukov, I.Y. Goryacheva, A. V. Sapelkin, Molecular nature of breakdown of the folic acid under hydrothermal treatment: a combined experimental and DFT study, Sci. Rep. 10 (2020) 1–6. https://doi.org/10.1038/s41598-020-76311-y.

[36] K. Wysoczanska, G. Sadowski, E.A. Macedo, C. Held, Toward Thermodynamic Predictions of Aqueous Vitamin Solubility: An Activity Coefficient-Based Approach, Ind. Eng. Chem. Res. 58 (2019) 7362–7369. https://doi.org/10.1021/acs.iecr.9b00742.

[37] I.R. Younis, M.K. Stamatakis, P.S. Callery, P.J. Meyer-Stout, Influence of pH on the dissolution of folic acid supplements, Int. J. Pharm. 367 (2009) 97–102. https://doi.org/10.1016/j.ijpharm.2008.09.028.

[38] G. Gocheva, N. Petkov, A. Garcia Luri, S. Iliev, N. Ivanova, J. Petrova, Y. Mitrev, G. Madjarova, A. Ivanova, Tautomerism in folic acid: Combined molecular modelling and NMR study, J. Mol. Liq. 292 (2019) 111392. https://doi.org/10.1016/j.molliq.2019.111392.

[39] C. Chen, J. Ke, X.E. Zhou, W. Yi, J.S. Brunzelle, J. Li, E.-L. Yong, H.E. Xu, K. Melcher, Structural basis for molecular recognition of folic acid by folate receptors, Nature. 500 (2013) 486–489. https://doi.org/10.1038/nature12327.

[40] A. Singh, N. Deshpande, N. Pramanik, S. Jhunjhunwala, A. Rangarajan, H.S. Atreya, Optimized peptide based inhibitors targeting the dihydrofolate reductase pathway in cancer, Sci. Rep. 8 (2018) 3190. https://doi.org/10.1038/s41598-018-21435-5.

[41] D. Braga, L. Chelazzi, F. Grepioni, L. Maschio, S. Nanna, P. Taddei, Folic Acid in the Solid State: A Synergistic Computational, Spectroscopic, and Structural Approach, Cryst. Growth Des. 16 (2016) 2218–2224. https://doi.org/10.1021/acs.cgd.6b00043.

[42] V.R.R. Cunha, V.R.L. Constantino, R.A. Ando, Raman spectroscopy and DFT calculations of para-coumaric acid and its deprotonated species, Vib. Spectrosc. 58 (2012) 139–145. https://doi.org/10.1016/j.vibspec.2011.12.007.

[43] V.R.R. Cunha, C.M.S. Izumi, P.A.D. Petersen, A. Magalhães, M.L.A. Temperini, H.M. Petrilli, V.R.L. Constantino, Mefenamic acid anti-inflammatory drug: Probing its polymorphs by vibrational (IR and Raman) and solid-state NMR spectroscopies, J. Phys. Chem. B. 118 (2014) 4333–4344. https://doi.org/10.1021/jp500988k.

[44] V.R.R. Cunha, P.A.D. Petersen, M.B. Gonçalves, H.M. Petrilli, C. Taviot-Gueho, F. Leroux, M.L.A. Temperini, V.R.L. Constantino, Structural, spectroscopic (NMR, IR, and Raman), and DFT investigation of the self-assembled nanostructure of pravastatin-LDH (layered double hydroxides) systems, Chem. Mater. 24 (2012) 1415–1425. https://doi.org/10.1021/cm202953y.

[45] A.D. Becke, Density- functional thermochemistry. III. The role of exact exchange, J. Chem. Phys. 98 (1993) 5648–5652. https://doi.org/10.1063/1.464913.

[46] A.D. Becke, Density- functional thermochemistry. IV. A new dynamical correlation functional and implications for exact- exchange mixing, J. Chem. Phys. 104 (1996) 1040–1046. https://doi.org/10.1063/1.470829.

[47] M.J. Frisch, G.W. Trucks, H.B. Schlegel, G.E. Scuseria, E. Al, Gaussian 16, Revision B.01, (2009).

[48] D. Mastropaolo, A. Camerman, N. Camerman, Folic acid: crystal structure and implications for enzyme binding, Science (80). 210 (1980) 334–336. https://doi.org/10.1126/science.7423195.

[49] M.P. Andersson, P. Uvdal, New Scale Factors for Harmonic Vibrational Frequencies Using the B3LYP Density Functional Method with the Triple-ζ Basis Set 6-311+G(d,p), J. Phys. Chem. A. 109 (2005) 2937–2941. https://doi.org/10.1021/jp045733a.

[50] G. Reibnegger, QT-AIM analysis of neutral pterin and its anionic and cationic forms, Pteridines. 25 (2014) 41–48. https://doi.org/10.1515/pteridines-2014-0005.

[51] K. Momma, F. Izumi, VESTA 3 for three-dimensional visualization of crystal, volumetric and morphology data, J. Appl. Crystallogr. 44 (2011) 1272–1276. https://doi.org/10.1107/S0021889811038970.

[52] J.A. Kaduk, C.E. Crowder, K. Zhong, Crystal structure of folic acid dihydrate, $C_{29}H_{29}N_2O_6(H_2O)_2$, Powder Diffr. 30 (2015) 52–56. https://doi.org/10.1017/S0885715614000815.

[53] R. Atluri, M.N. Iqbal, Z. Bacsik, N. Hedin, L.A. Villaescusa, A.E. Garcia-Bennett, Self-Assembly Mechanism of Folate-Templated Mesoporous Silica, Langmuir. 29 (2013) 12003–12012. https://doi.org/10.1021/la401532j.

[54] O. Ostroverkhova, Organic Optoelectronic Materials: Mechanisms and Applications, Chem. Rev. 116 (2016) 13279–13412. https://doi.org/10.1021/acs.chemrev.6b00127.

[55] N.J. Hestand, F.C. Spano, Expanded Theory of H- and J-Molecular Aggregates: The Effects of Vibronic Coupling and Intermolecular Charge Transfer, Chem. Rev. 118 (2018) 7069–7163. https://doi.org/10.1021/acs.chemrev.7b00581.

[56] G. Li, D. Magana, R.B. Dyer, Photoinduced electron transfer in folic acid investigated by ultrafast infrared spectroscopy, J. Phys. Chem. B. 116 (2012) 3467–3475. https://doi.org/10.1021/jp300392a.

[57] A. Tyagi, A. Penzkofer, Fluorescence spectroscopic behaviour of folic acid, Chem. Phys. 367 (2010) 83–92. https://doi.org/10.1016/j.chemphys.2009.10.026.

[58] H.B. Fu, J.N. Yao, Size effects on the optical properties of organic nanoparticles, J. Am. Chem. Soc. 123 (2001) 1434–1439. https://doi.org/10.1021/ja0026298.

[59] A. Tiwari, B. Raj, Reactions and Mechanisms in Thermal Analysis of Advanced Materials, 1st ed., Wiley-Scrivener, 2015. https://doi.org/10.1002/9781119117711

[60] A. Vora, A. Riga, K. Alexander, Processes to Identify the Degradation Mechanism of a Solid which Appears to Undergo a Complex Reaction: Folic Acid, Instrum. Sci. Technol. 30 (2002) 193–203. https://doi.org/10.1081/CI-120003899.

[61] C. Bonechi, A. Donati, R. Lampariello, S. Martini, M.P. Picchi, M. Ricci, C. Rossi, Solution structure of folic acid: Molecular mechanics and NMR investigation, Spectrochim. Acta - Part A Mol. Biomol. Spectrosc. 60 (2004) 1411–1419. https://doi.org/10.1016/j.saa.2003.08.007.

[62] N.B. Colthup, L.H. Daly, S.E. Wiberley, Introduction to Infrared and Raman Spectroscopy, 3rd ed., Academic Press, 1990.

[63] B. Profantová, V. Profant, V. Zíma, V. Kopecký, L. Bednárová, C. Zentz, V. Baumruk, P.Y. Turpin, J. Štěpánek, Protonation effect of tyrosine in a segment of the SRF transcription factor: A combined optical spectroscopy, molecular dynamics, and density functional theory calculation study, J. Phys. Chem. B. 117 (2013) 16086–16095. https://doi.org/10.1021/jp4099864.

[64] K.B. Beć, J. Grabska, M.A. Czarnecki, C.W. Huck, M.J. Wójcik, T. Nakajima, Y. Ozaki, IR Spectra of Crystalline Nucleobases: Combination of Periodic Harmonic Calculations with Anharmonic Corrections Based on Finite Models, J. Phys. Chem. B. 123 (2019) 10001–10013. https://doi.org/10.1021/acs.jpcb.9b06285.

[65] A. Barth, Infrared spectroscopy of proteins, Biochim. Biophys. Acta - Bioenerg. 1767 (2007) 1073–1101. https://doi.org/10.1016/j.bbabio.2007.06.004.

[66] B. Sjöberg, S. Foley, B. Cardey, M. Enescu, An experimental and theoretical study of the amino acid side chain Raman bands in proteins, Spectrochim. Acta - Part A Mol. Biomol. Spectrosc. 128 (2014) 300–311. https://doi.org/10.1016/j.saa.2014.02.080.

[67] L. Li, T. Cai, Z. Wang, Z. Zhou, Y. Geng, T. Sun, Study on molecular structure, spectroscopic investigation (IR, Raman and NMR), vibrational assignments and HOMO–LUMO analysis of L-sodium folinate using DFT: A combined experimental and quantum chemical approach, Spectrochim. Acta Part A Mol. Biomol. Spectrosc. 120 (2014) 106–118. https://doi.org/10.1016/j.saa.2013.10.011.

[68] C.K. Nandi, M.K. Hazra, T. Chakraborty, Vibrational coupling in carboxylic acid dimers, J. Chem. Phys. 123 (2005) 124310. https://doi.org/10.1063/1.2039084.

[69] R.P. Lopes, M.P.M. Marques, R. Valero, J. Tomkinson, L.A.E.B. de Carvalho, Guanine: A Combined Study Using Vibrational Spectroscopy and Theoretical Methods, Spectrosc. An Int. J. 27 (2012) 273–292. https://doi.org/10.1155/2012/168286.

[70] J.J. Castillo, C.E. Rozo, L. Bertel, T. Rindzevicius, S.C. Mendez‐ Sanchez, F.M. Ortega, A. Boisen, Orientation of Pterin-6-Carboxylic Acid on Gold Capped Silicon Nanopillars Platforms: Surface Enhanced Raman Spectroscopy and Density Functional Theory Studies, J. Braz. Chem. Soc. 2 (2015) 123–125. https://doi.org/10.5935/0103-5053.20150352.

[71] R. Świsłocka, M. Samsonowicz, E. Regulska, W. Lewandowski, Molecular structure of 4-aminobenzoic acid salts with alkali metals, J. Mol. Struct. 792–793 (2006) 227–238. https://doi.org/10.1016/j.molstruc.2005.10.060.

[72] P. Ilich, C.F. Hemann, R. Hille, Molecular Vibrations of Solvated Uracil. Ab Initio Reaction Field Calculations and Experiment, J. Phys. Chem. B. 101 (1997) 10923–10938. https://doi.org/10.1021/jp9706285.

[73] A. Andrejeva, A.M. Gardner, W.D. Tuttle, T.G. Wright, Consistent assignment of the vibrations of symmetric and asymmetric para-disubstituted benzene molecules, J. Mol. Spectrosc. 321 (2016) 28–49. https://doi.org/10.1016/j.jms.2016.02.004.

[74] B. Hernández, Y.-M. Coïc, F. Pflüger, S.G. Kruglik, M. Ghomi, All characteristic Raman markers of tyrosine and tyrosinate originate from phenol ring fundamental vibrations, J. Raman Spectrosc. 47 (2016) 210–220. https://doi.org/10.1002/jrs.4776.

[75] M. Ghosh, S. Gayen, K.K. Dey, An atomic resolution description of folic acid using solid state NMR measurements, RSC Adv. 10 (2020) 24973–24984. https://doi.org/10.1039/D0RA03772A.

[76] H.T.A. Cheung, B. Birdsall, T.A. Frenkiel, D.D. Chau, J. Feeney, Carbon-13 NMR determination of the tautomeric and ionization states of folate in its complexes with Lactobacillus casei dihydrofolate reductase, Biochemistry. 32 (1993) 6846–6854. https://doi.org/10.1021/bi00078a007.